Optimizing the precision of infrared measurements using the Eppley pyrgeometer model PIR

Joseph J. Michalsky[1], John A. Augustine[1], Emiel Hall[1], and Benjamin R. Sheffer[1, 2]

[1]Global Monitoring Laboratory, National Oceanic and Atmospheric Administration, Boulder, Colorado 80305, USA
[2]Cooperative Institute for Research in Environmental Sciences, University of Colorado, Boulder, Colorado 80309, USA

Correspondence: Joseph Michalsky (joseph.michalsky@noaa.gov)

Abstract. The Eppley Model PIR is widely used for thermal infrared wavelength (3.5-50 μm) measurements of the downwelling and upwelling radiation from the atmosphere and surface, respectively. The field of view of the instrument is 2π steradians with a receiver that has an approximate cosine response. In this paper we examine four equations in the literature that have been used to process field PIR measurements and to transfer calibration from standards to field units that are used in network operations. We begin with a discussion of various equations used to convert the resistance of the YSI 44031 thermistors used in PIRs for temperature measurements of the body (or case) and dome that are used to derive an incoming irradiance. We then use the four distinct equations for the transfer of the calibration from standards to field instruments. Clear choices in the equations to use for calibration and transfer of calibration to field PIRs emerge from this study.

1. Introduction

The Eppley model PIR pyrgeometer was developed to measure longwave thermal infrared (IR) radiation emitted by the sky and surface. It came equipped with a battery-powered circuit to compensate for the radiation emitted by the body (or case) so the net signal from the instrument is a measure of actual incoming infrared radiation. Most users of this instrument do not use the battery-powered circuit, but, instead, use the temperatures from two thermistors connected to the body of the instrument and dome, along with the thermopile output, to calculate the infrared irradiance signal.

Fig. 1 illustrates the major incoming and outgoing IR irradiance at the thermopile surface. To derive L, the incoming IR radiation from the hemisphere outside the instrument, radiative equilibrium of the instrument must be defined. To do that, the first three IR components in Fig. 1 (labeled 1, 2, 3) are set equal to fourth component (labeled 4). Considering those components, Albrecht and Cox (1977) formulated Eq. 1 for the externally received infrared radiation as,

$$L = U_{thermopile}(c_1 + c_2 T_B^3) + \varepsilon_o \sigma T_B^4 - k\sigma(T_D^4 - T_B^4), \quad (1)$$

where L is the external incoming infrared irradiance, $U_{thermopile}$ is the voltage measured across the thermopile, T_B and T_D are the body and dome temperatures in degrees K, σ is the Stefan-

Deleted: methodology

Deleted: was

Commented [JA1]: Joe,
You should say why the circuit is not typically used.

Deleted: incoming

Deleted: infrared

Deleted: s

Deleted: ,

Deleted: terms

Deleted: term

Deleted: produced this equation

Deleted: from their analysis

Formatted: Right: 0.25"

Boltzmann constant, ε_o is the emissivity of the detector, and c_1, c_2, and k are constants to be determined in calibration.

Deleted: during

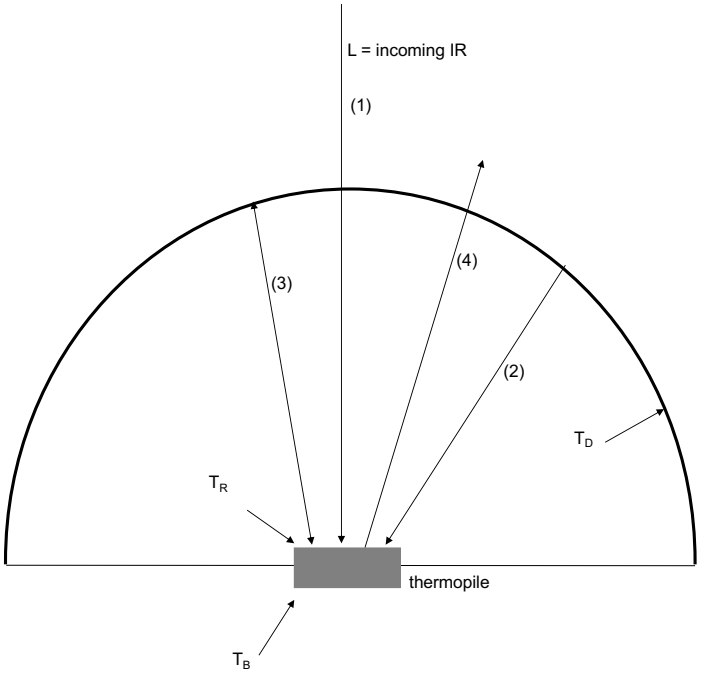

Figure 1. Schematic for the major incoming and outgoing infrared rays that are considered in calculating the incoming infrared, where the top of the dark rectangular area is the receiving surface/thermopile and surrounding arc is the reflective dome of the PIR. The interior of the dome is coated with a filter that allows IR radiation to pass through and the outer surface reflects/rejects all impinging solar radiation. T_R, T_B, and T_C are the receiver surface, the body, and the dome temperatures, respectively, in degrees K.

In practice Albrecht and Cox (1977) dropped the $c_2 T_B^3$ term as negligible relative to the c_1 term and set the emissivity of the body of the instrument ε_o to 1 yielding this commonly expressed form of their equation

$$L = \frac{U_{thermopile}}{C} + \sigma T_B^4 - k\sigma(T_D^4 - T_B^4), \quad (2)$$

where c_1 has been replaced by $1/C$.

Formatted: Right: 0.25"

Philipona et al. (1995), however, used Eq. (1) in its entirety, but to compare symbolically to Eq. (2) it is written as:

$$L = \frac{U_{thermopile}}{C}(1 + k_1\sigma T_B^3) + k_2\sigma T_B^4 - k_3\sigma(T_D^4 - T_B^4), \quad (3)$$

where the T_B^3 term in Eq. (1) is retained, the emissivity of the body is k_2, and k_3 is the same as k in Eq. (2). All constants, C, k_1, k_2, and k_3, are determined in calibration.

Payne and Anderson (1999) used the functional form of Eq. (2), but substituted T_R for the T_B, where T_R is the empirically computed approximate temperature of the receiving surface rather than the measured body temperature, as illustrated in Fig. 1. Thus,

$$L = \frac{U_{thermopile}}{C} + \sigma T_R^4 - k\sigma(T_D^4 - T_R^4). \quad (4)$$

Payne and Anderson (1999) calculated T_R using Eq. 5

$$T_R = T_B + 0.694 \cdot U_{thermopile} \quad (5)$$

where $U_{thermopile}$ is in millivolts, and the emissivity ε_o is set to unity.

Reda et al. (2002) used a form similar to Eq. (4)

$$L = k_0 + \frac{U_{thermopile}}{C} + k_2\sigma T_R^4 - k_3\sigma(T_D^4 - T_R^4), \quad (6)$$

where the instrument body emissivity k_2 is derived during calibration and a constant term k_0 is introduced. T_R is nearly the same as Eq. (5) with 0.704 replacing the constant 0.694.

The organization of this paper is as follows. Because accurate internal thermistor temperatures are critical to pyrgeometer IR measurements, we first examine various versions of the Steinhart-Hart equation that have been used to convert the Y44031 thermistor resistance to the temperature of the PIR body and dome. We then calibrate three test PIRs by transferring the calibrations of three standard PIRs that were calibrated at the World Radiation Center (WRC) in Davos, Switzerland using the World Infrared Standard Group (WISG). Comparisons are then made between the mean irradiance of the three standard PIRs and the computed irradiance from the test PIRS using the four different forms of the original Albrecht and Cox (1977) formula, i.e., Eq. (1). Boxplots are used to demonstrate the level of agreement between the standards and test PIRs for the various formulations. A clear conclusion with regard to the preferred technique to use for calibration and field measurements is suggested in the summary section.

2. PIR Temperature Measurements

Deleted: is to be determined in calibration
Formatted: Font: Italic
Formatted: Font: Italic, Subscript
Formatted: Font: Italic
Formatted: Font: Italic, Subscript
Formatted: Font: Italic
Formatted: Font: Italic
Formatted: Font: Italic, Subscript
Deleted: a calculation of the
Deleted: In their paper
Deleted: this equation
Deleted: with
Deleted: In this paper
Deleted: forms of
Deleted: measured in
Deleted: on the
Deleted: using
Deleted: received their calibrations
Deleted: , where the World Infrared Standard Group (WISG) is used for calibration
Deleted:
Deleted: with
Deleted: our
Deleted: to be
Deleted: calibrated over several days using
Deleted: are used to
Deleted: newly calibrated pyrgeometers
Deleted: s
Deleted: s
Deleted: of this paper
Formatted: Right: 0.25"

The two temperature measurements in the Eppley PIR pyrgeometer are made using the YSI 44031 thermistor. Steinhart and Hart (1968) found that a cubic fit of temperature to the log of measured resistance matched many thermistor data points over a wide temperature range. Their equation is

$$\frac{1}{T} = a + b \cdot \ln(R) + 0 \cdot \ln(R)^2 + d \cdot \ln(R)^3, \quad (7)$$

where T is in degrees K and R is in ohms or kiloohms. Note that the squared term has a zero coefficient. Coefficients *a, b,* and *d* differ for the same thermistor depending on whether ohms or kiloohms are used and depending on the temperature range over which the fit is made.

Fig. 2 is a plot of four independently-derived fits to the YSI 44031 thermistor data. The y-axis is the temperature estimate based on the fit minus the tabulated thermistor data to which the fit is made. The red and blue lines are least squares linear fits to Eq. 7 (no squared term) over the range of -50 to 50°C in one-degree increments. Resistance in ohms is used for the red curve. If a full cubic (include the squared term) is fit to the tabulated data in kiloohms, then similar agreement is obtained (blue curve). Interestingly, if the fit with the full cubic is made to ohms, rather than kiloohms, the agreement to the red curve is identical (not shown). Two fits found in the literature to different temperature ranges (McArthur, 2005; Gröbner, 2025) are also plotted in Fig. 2. The Physikalisch-Meteorologisches Observatorium Davos (PMOD) fit (Gröbner, 2025; green) is over a -30 to +40 C range. If the Baseline Surface Radiation Network (BSRN) (McArthur, 2005; gray curves) coefficient *a* is modified slightly from the published 0.0010295 to 0.0010293, as shown in the legend, then an improved fit (upper gray curve) is obtained that agrees well with the others in Fig. 2. Although the differences among the various fits in Fig. 2 are small, it is obvious that those over the -50 to 50°C range give the better result, and therefore the red curve used to compute PIR temperatures in the data analyzed here.

Deleted: in

Deleted:

Deleted: fit

Commented [JA2]: This phrase may cause confusion. The reader may think that each thermistor has its own coefficients. I suggest removing "for the same thermistor"

Deleted: The c

Commented [JA3]: I removed "–50 t0 50" here all because not all of the fits shown are for that range

Deleted:

Deleted: from -50 to 50 C in one-degree increments

Deleted: The least-squares fit to Eq. (7) is

Deleted: the red line if ohms are used.

Deleted: used to fit

Deleted: line

Deleted: By the way

Deleted: Next, t

Deleted: estimates

Deleted: (McArthur, 2005; Gröbner, 2025) that are fit to the resistance in ohms

Deleted: ;

Commented [JA4]: Do you know the temperature range Bruce used?

Formatted: Right: 0.25"

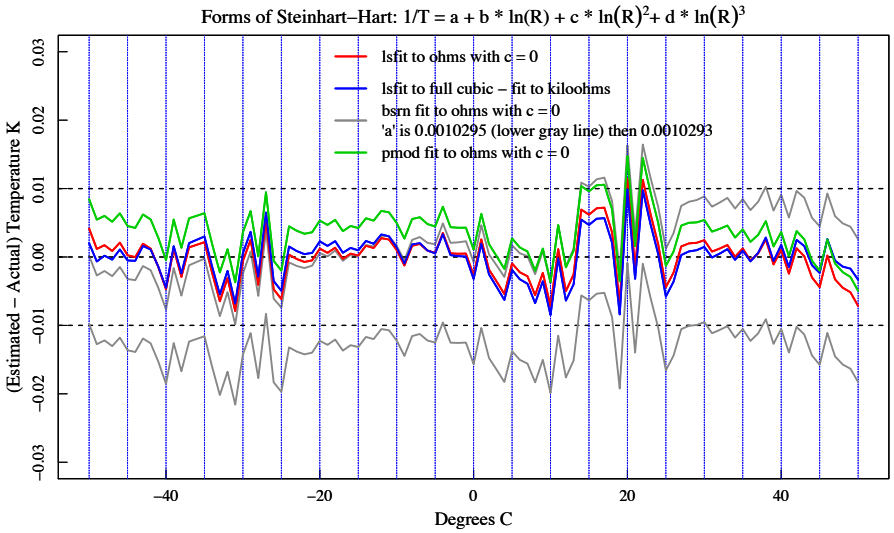

Figure 2. Four independent fits using forms of Eq. (7) to the YSI 44031 tabulated data after subtraction of the tabulated data over the range -50 to 50 C. Similar agreement among all four ensues after the small change to the BSRN constant *a*.

3. Four Methods of PIR Calibration Transfer

In this section, we apply Eq. (2), (3), (4), and (6) to examine how well each performs in transferring calibrations from our "standard" PIRs, that were calibrated against the world reference at PMOD, to field PIRs. The three standard PIRs were calibrated at the World Radiation Center (WRC) in Davos, Switzerland in 2018, 2022, and 2024. (https://www.pmodwrc. ch/en/world-radiation-center-2/irs/wisg/). Each was returned with two sets of coefficients, one for Eq. (2) and one for Eq. (3).

To transfer the standards' calibration to field radiometers, the standard and test PIRs are arranged side-by-side on an outdoor observing platform and run for a week or more. There are no significant obstructions surrounding the platform. Fig. 3 is an example of one such period. On the left are the three standards' output with the WRC-supplied Philipona et al. (1995) calibration coefficients applied. On the right is output from the same standards, but using the WRC-supplied Albrecht and Cox (1977) coefficients. Agreement among the three on the left is very good because the last PIR readings (green) overplot the first two (black and red). Agreement on the right is nearly as good but with some underestimation by PIR 32909F3 (red dots).

Deleted: of Calibration
Deleted: Three
Deleted:
Deleted: are used for our standards to calibrate the field units. These three
Deleted: sent for calibration
Deleted: to
Deleted: d,
Deleted: the years
Deleted: in
Deleted: PIR
Deleted: set
Deleted: T
Deleted: three
Deleted: s
Deleted: , typically,
Deleted: two or three
Deleted: to be calibrated
Deleted: horizontal
Deleted: ,
Deleted: with
Deleted: , for a week or more
Deleted: calibration
Deleted: s
Deleted: using
Deleted: ,
Deleted: (
Deleted: ,
Deleted: are
Deleted:
Deleted: ,
Deleted: ,
Deleted: applied
Deleted: The legend values are the serial numbers of the three PIRs calibrated at WRC. The a
Deleted: appears
Deleted: The a
Deleted: for
Deleted: the
Formatted: Right: 0.25"

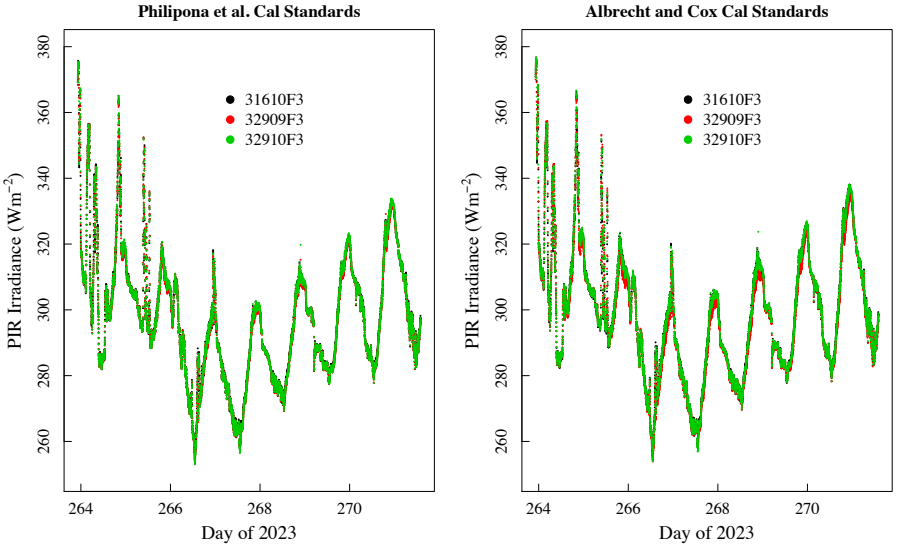

Figure 3. Computed IR irradiance from our three standard PIRs (serial numbers in the legend) using coefficients provided by WRC are overplotted with the Philipona et al. coefficients on the left and the Albrecht and Cox coefficients on the right. This demonstrates the agreement among the standards using the two methods. The length of the period shown is typical for our runs.

Before comparing results from Eq. (2), (3), (4), and (6), we first compare results from only Albrecht and Cox (Eq. 2) and Philipona (Eq. 3) for which the WRC provides coefficients. In this test, the mean IR irradiance of the three standards is compared to computed IR from a test PIR. The test PIR has been calibrated by transferring the calibration of the three standards. The least-squares fitting technique to determine the calibration coefficients for the test instrument uses a robust technique in the R language (MASS::rlm) that de-weights outliers to reduce the effects of noisy, rain-contaminated. i.e., outlier, data.

In Figure 4, boxplots are used to compare the performance of the two calibration methods applied to the standards at the WRC. The "box" in those plots contain 50% of the data, and the lines extending from the top and bottom of the box, or "whiskers," include about 95% for normally distributed data. In the top-left panel of Fig. 4 the three standards use the WRC-provided Albrecht and Cox (1977) coefficients, and the average of the three standards is compared to coincident test PIR (SN 23215F3) data, also calculated using Albrecht and Cox (1977). The boxplot summarizes those differences over the entire calibration period for PIR 23215F3. The boxplot on the top right summarizes differences following the same procedure, but using Philipona et al. (1995) coefficients for the standards (WRC-provided) and for the test PIR. Comparing the top panels of Fig. 4, the one on the right, where Philipona coefficients are used exclusively, has a smaller box, and a median nearer to zero compared to the panel on the left where Albrecht and Cox was used exclusively.

Deleted: O
Deleted: all
Deleted: ,
Deleted: ,
Deleted: using
Deleted: (
Deleted:
Deleted: sets of
Deleted: for the standards we are using
Moved (insertion) [2]
Deleted: (PIR 23215)
Deleted: cloud
Deleted:
Deleted: (top-left) our
Deleted: and calculate an
Deleted: for
Deleted: . From this we subtract the PIR value
Deleted: that was
Deleted: after calibration
Deleted: this
Deleted: coefficients
Deleted: The
Deleted: on the left indicates
Deleted: ¶
Deleted: in Fig. 3
Deleted: indicates
Deleted: WRC-provided
Deleted: 23215 measurements after calibration using¶ these standards
Moved up [2]: The least-squares fitting technique to determine the calibration coefficients for the test instrument (PIR 23215) uses a robust technique in the R language
Moved (insertion) [1]
Deleted: .
Deleted: left and right
Deleted: the panel
Deleted: t
Deleted: ,
Deleted: which contains 50% of the data, shorter whis ... [1]
Deleted: that is
Deleted: .
Formatted: Right: 0.25"

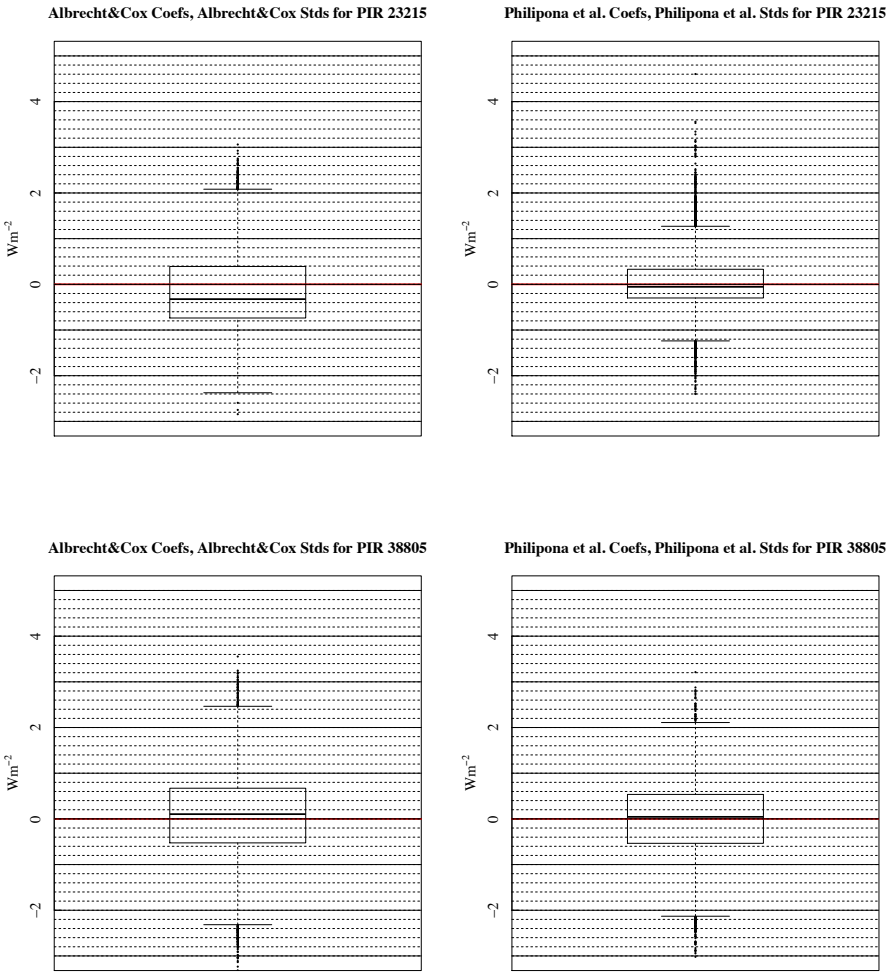

Figure 4. (top) Boxplots of the differences between applying Albrecht and Cox (1977) calibrations and applying Philipona et al. (1995) calibrations for PIR 23215. Note the differences in box widths, whisker lengths, and median values. (bottom) Boxplots for a different PIR (38805) that was calibrated at the same time as the one in Fig. 4 (top).

Formatted: Right: 0.25"

The bottom panels of Fig. 4 show the same comparison for another test PIR (SN 38805F3). The same comments apply, with the Philipona et al. (1995) calibrated data (right) giving smaller spread in the box and whiskers, and the median nearer zero, while there is more spread in the left panel where Albrecht and Cox (1977) is used. However, differences in the lower panels of Fig. 4 are greater than those in the top panels. The calibration data for these two test instruments were collected concurrently, which suggests that the disparity arises from inherent differences in the instruments themselves. We studied a total of six instruments from two distinct calibration periods in this way and found that in every case using the Philipona et al. (1995) form (Eq. 3) gave slightly better results than the formulation of Albrecht and Cox (1977) (Eq. (2).

Next, we compare results from all four equations (2), (3), (4), and (6) for the same two test PIRs. Since Fig. 4 suggests that the Philipona et al. (1995) Eq. (3) produces better results than Albrecht and Cox (1977) Eq. (2), we use Philipona coefficients provided by WRC to compute IR irradiance for the standards and average them as "truth" for all of the comparisons. For both test PIRs (top and bottom), Fig. 5 shows the last boxplot on the right (Philipona) to give the best results followed closely by the adjacent boxplot (Reda).

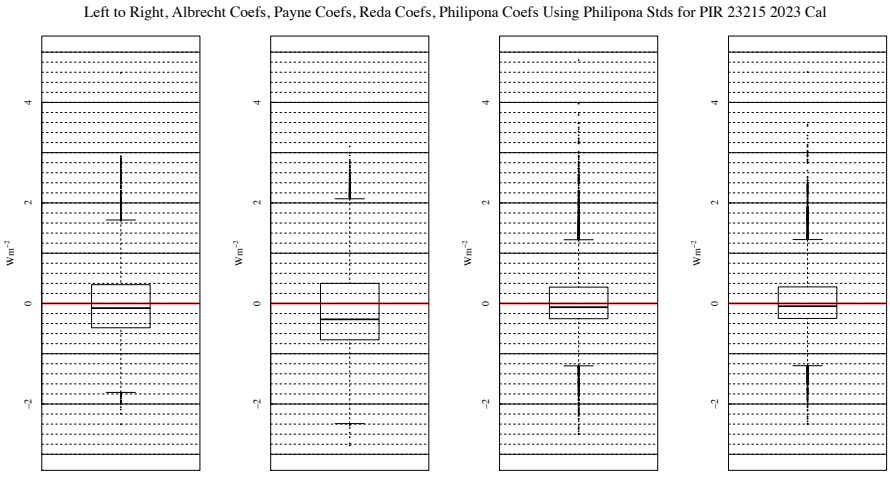

Albrecht = Albrecht and Cox (1977); Payne = Payne and Anderson (1999); Reda = Reda et al. (2002); Philipona = Philipona et al. (1995)

Moved up [1]: Comparing the left and right panels, the panel on the right has a smaller box, which contains 50% of the data, shorter whiskers, which for a normal distribution includes about 95% of the data, and a median that is nearer zero compared to the panel on the left.

Deleted: In Fig. 4 (bottom)

Deleted:

Deleted: t

Deleted: for

Deleted: than the left panel (

Deleted: ,

Deleted: the

Deleted: Fig. 4

Deleted: (top).

Deleted: s

Deleted: of

Deleted: . This

Deleted: differences

Deleted: studied

Deleted: that

Deleted:)

Deleted: using boxplots for the comparison

Deleted: will

Deleted: Eq. (3)

Deleted: for our

Deleted: these

Deleted: Fig. 5

Formatted: Right: 0.25"

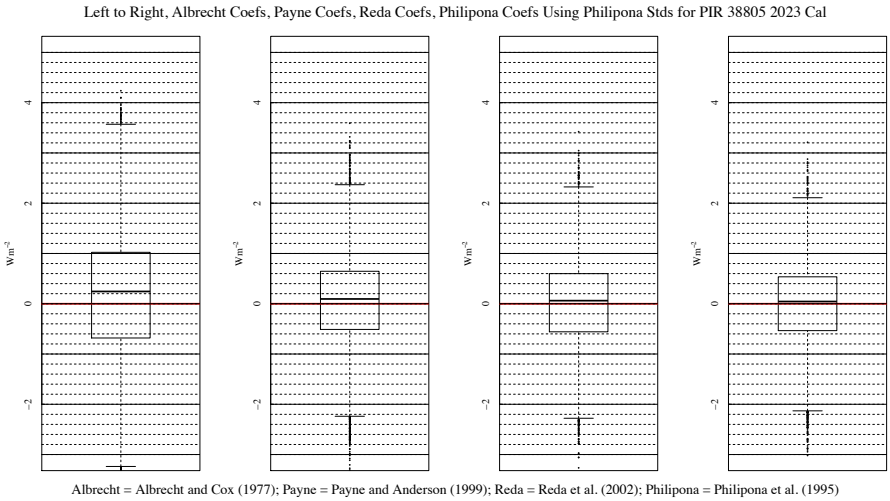

Figure 5. Boxplots of differences using the WRC's Philipona et al. (1995) coefficients for the standards and calibrated PIRs to this standard using the four equations to calculate incoming infrared. Top is for PIR 23215 and bottom is PIR 38805 as in Fig. 4. Compare box widths, whisker lengths, and medians.

Note that the leftmost boxplots of Fig. 5 are similar to the leftmost boxplots in Fig. 4, with better results for PIR 23215F3 (top) than PIR 38805F3 (bottom). Similar results were obtained for the other four PIRs tested (not shown) with the best results always obtained with the Philipona et al. (1995) formulation, followed closely by the Reda et al. (2002) method. In one case out of the six the Payne and Anderson (1999) formula performed ever so slightly better than the Reda et al. (2002) formula (not shown).

4. Precision of the PIR standards

Four formulae in the literature for calculating incoming infrared with an Eppley model PIR pyrgeometer were tested to sort out the precision of transferring calibrations from standards to field deployed PIRs. Calibrations of the same three standards were made at the WRC in 2018, 2022, and 2024. For all three of these independent calibration events, coefficients for the Albrecht and Cox (1977) and Philipona et al. (1995) forms of the PIR processing equation for calculating infrared were provided. Here we look at the repeatability of those biennial calibration events.

Our calibration season typically runs from late Spring to early Fall. Therefore, our three PIR standards experience roughly six months of exposure to the weather each year. In Fig. 6 differences from applying three sets of WRC Philipona calibration coefficients from 2018, 2022,

Deleted: is
Deleted: the
Deleted: the top (
Deleted: ,
Deleted: but worse results for the bottom (
Deleted: In these two cases the standard used was calibrated with Philipona et al. (1995) coefficients.
Deleted: for all six
Moved down [3]: 4. Discussion and Summary¶
¶
Moved (insertion) [3]
Deleted: Discussion and Summary
Deleted: that are
Deleted: find
Deleted: available in
Deleted: pyrgeometers
Deleted: C
Deleted: incoming
Deleted: by the WRC
Deleted: includes
Deleted: , Summer, and
Deleted: the
Deleted: in
Deleted: (
Formatted: Right: 0.25"

and 2024 to the same dataset (that used for Fig 3) are summarized. For example, calibrations from 2018 and 2022 were applied to a common dataset and differences in irradiance for each minute were tallied and summarized in boxplots. Differences for all permutations are mostly within 1 Wm^{-2} and suggest that errors from applying one of the WRC calibrations from any of the three calibration years to any year would be less than the uncertainty of the WRC calibrations themselves. This suggests that the Eppley PIR is very stable and suitable for monitoring long-term changes in the thermal infrared.

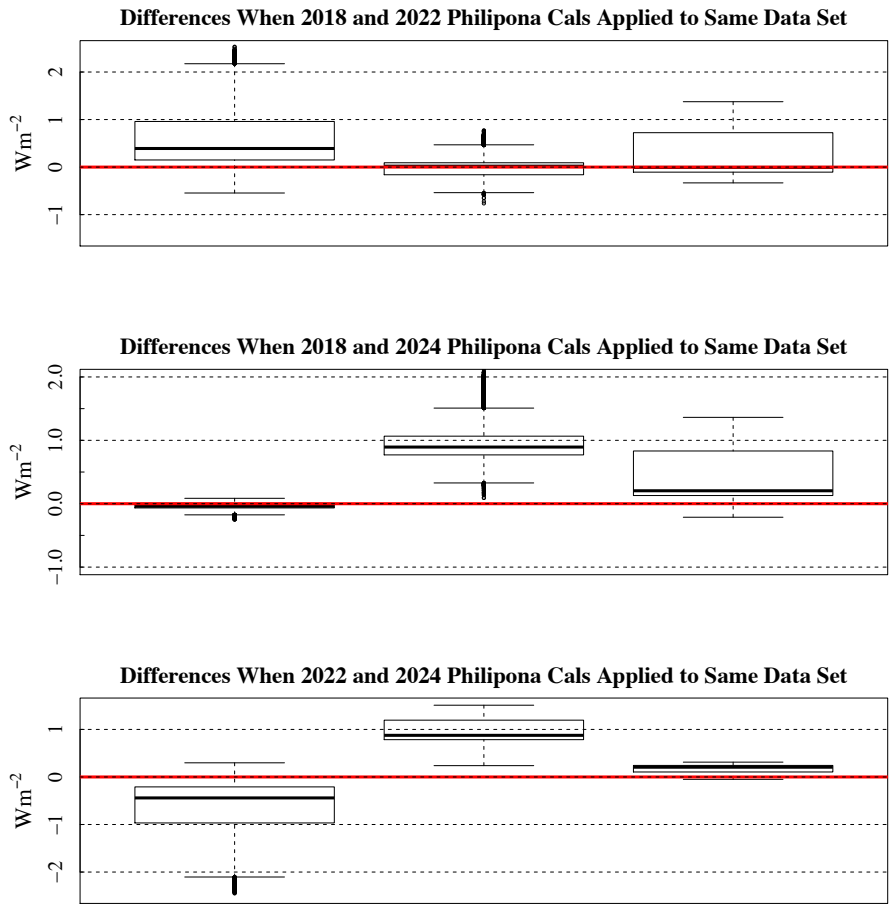

Figure 6. Comparisons of three sets of Philipona et al. (1995) calibration coefficients provided by the WRC in 2018, 2022, and 2024 applied to the same data set as in Fig. 3 for the three PIRs

Deleted:)
Deleted: calibration run
Deleted: as in Fig. 3
Deleted: shown as boxplots for our three standards
Deleted: with serial numbers in the subtitle
Deleted: The d
Deleted: small enough
Formatted: Superscript
Deleted: equivalent to within
Formatted: Right: 0.25"

used as standards with serial numbers in the subtitle. The medians are all within 1 Wm^{-2} and most are withing 0.4 Wm^{-2}.

In section 3 the average output of the three standards is used to derive new calibration coefficients for each test PIR. Using those new calibrations, the test instrument measurements are compared to the standards' average over the entire calibration period. For the left panels in Fig. 7 we use Philipona et al. (1995) coefficients for the standards to calibrate the three test PIRs (serial numbers shown at the top of each subplot). We apply those new calibrations and subtract the results from the standards' average for each minute and summarize the distribution of differences in boxplots. Therefore, the leftmost panels of Fig. 7 replicates the rightmost panels of Figs. 4 and 5. This is not an independent test of the reliability of the calibration because the same dataset is used for calibration and verification.

To test new calibrations with an independent dataset, the time series in Figure 3 is divided in half. The middle panels of Fig. 7 use the first half of the data in Fig. 3 to derive a calibration and the second half of the data to validate the new calibration against the standards' average. Then, we reverse this process using the second half of the Fig. 3 data for calibrating and the first half to validate. If we examine the time series in Fig. 3, it is apparent that the first half of the data stream is noisier than the second half. Using the first half of the data to calibrate and applying to the second half and vice versa is likely responsible for the offsets in the medians, but the offsets are less than a Wm^{-2}. Note that when the smoother data of the second half are used to validate (middle boxplots) the differences have a smaller spread. Alternately, when the noisier first half data (rightmost boxplots) are used to validate, the differences have a larger spread. Examining the top, middle, and bottom plots, there are differences inherent in the instruments themselves since boxplots are not replicated from PIR to PIR. Attribution to the instruments themselves here is warranted because the standards and test data used for Fig. 7 were collected simultaneously.

Deleted: d…output of the three standards was …s used to derive new the …alibration coefficients for each test PIR being calibrated…;…using …sing this …hose new calibrations, the test instrument measurements were …re then …ompared to the standards' average over the entire calibration period. This was not an independent test of the reliability of the calibration. …or the left panels iI… Fig. 7 ww… use Philipona et al. (1995) coefficients for the standards to derive the calibration…alibrate for …he the three test PIRs with the …serial numbers shown at the top of of each subplot).;…We applythen with …that …hose new calibrations we…nd subtract the results from the standards' average the derived infrared for the calibrated each minute and summarize the distribution of differences in boxplots.;…Tt…erefore, the leftmost panels of Fig. 7 replicates the rightmost panels of Figs. 5 … and 6 ... [2]

Deleted: In the…he next …iddle panels of Fig. 7 we used…the first half of the data in Fig. 3 to derive a calibration and used …he second half of the data to test validate this …he new calibrated …alibration instrument against the standards' average in the second half… Finally…hen, we reverse this process using the second half of the Fig. 3 data for calibrating the instrument …nd the first half to test this calibrated instrument…alidate against the standards… ¶ ¶ ... [3]

Formatted: Right: 0.25"

Left to Right: Full Cal Period; 1st Half Used for Cal, Applied to 2nd Half; and Vice Versa for PIR 23215

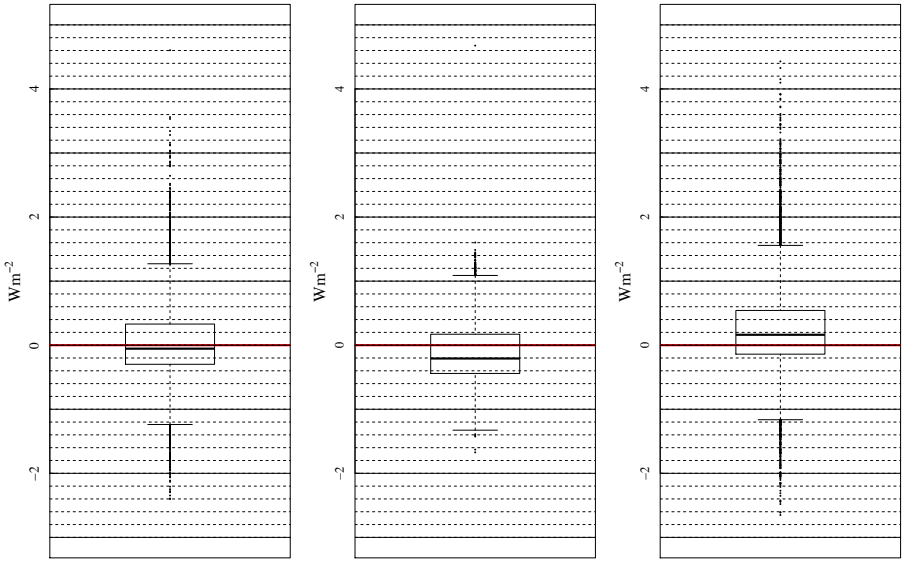

Left to Right: Full Cal Period; 1st Half Used for Cal, Applied to 2nd Half; and Vice Versa for PIR 28139

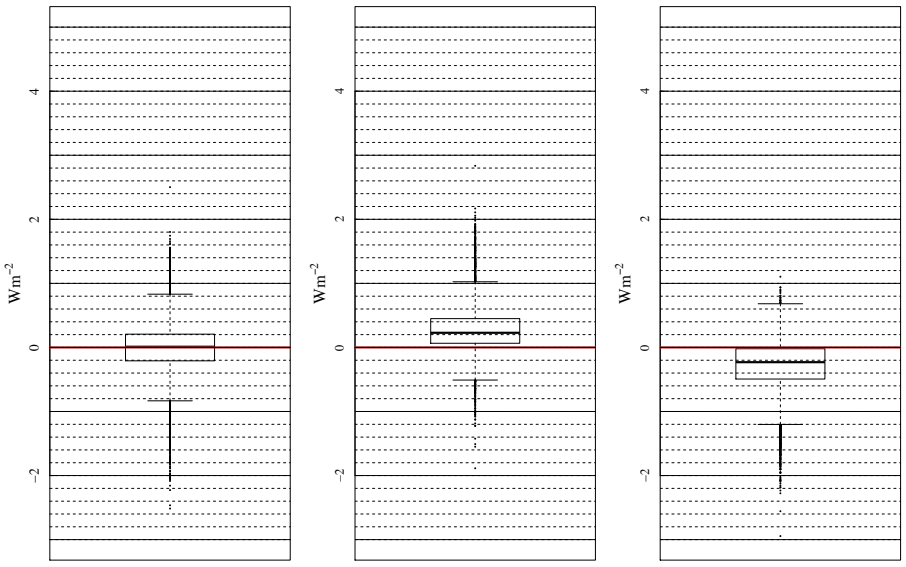

Formatted: Right: 0.25"

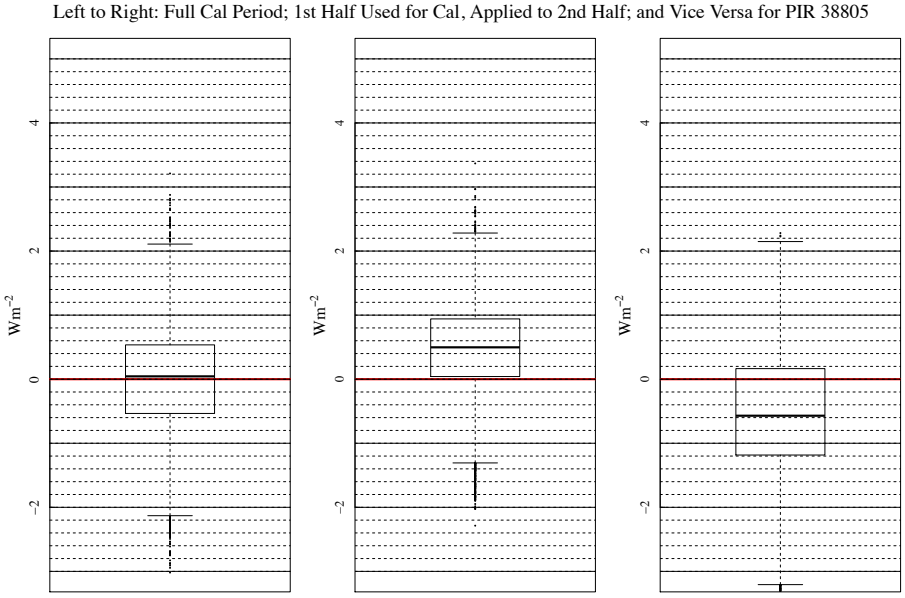

Figure 7. The leftmost panel uses the entire period in Fig. 3 to calibrate the named PIR and then compare the calibrated PIR data to the standards averaged. The middle panel uses the first half of the period to calibrate and then compares the second half using these calibrations. The rightmost panel reverses this using the second half of the period for calibration and the first half for comparisons.

5. Summary and Conclusions

In this paper we investigate four formulations for converting raw voltage and body and dome temperature measurements of an Eppley pyrgeometer, model PIR to thermal infrared irradiance. These methods are described in Albrecht and Cox (1977), Philipona et al. (1995), Reda et al. (2002) and Payne and Anderson (1999). All are slight variations of the original formulation of Cox and Albrecht (1977). Because the temperature measurements are so critical to the calculations, we also investigate various fits that have been applied to the Steinhart and Hart (1968) equation that converts thermistor-measured resistance to temperature.

Regarding the computation of thermistor temperatures, we found that fitting the manufacturer-supplied table of resistance and temperature (1°C interval) to the range -50° to 50°C provides the least variability as opposed to fits to shorter temperature ranges. Although, differences of the fit to the provided data are < 0.01°C, regardless of the range used. Based on this result, we conclude that differences in thermistor temperature calculations do not have a significant impact on PIR measurements.

Formatted: Font: Bold
Formatted: Font: Bold
Formatted: Font:
Formatted: Right: 0.25"

The three standard PIRs that we use to transfer calibrations from the world standard are sent biennially to be calibrated against the world infrared standard group (WISG) at the World Radiation Center at Davos, Switzerland. They are returned with calibration coefficients for the Albrecht and Cox (1977) and Philipona (1995) methods, but the Albrecht and Cox coefficients are for the shortened form of the equation reported in their 1977 paper. Comparing the application of the two methods to the standard PIRs revealed that the Philipona (1995) method is more accurate and less noisy than the Albrecht and Cox method, however, the differences are small. Comparisons were also made among three distinct WRC calibration results for the standard PIRs in 2018, 2022, and 2024. These showed that the three standard PIRs are stable, with the calibration coefficients changing minimally between calibration eras, and differences in irradiance calculations among the separate calibrations being within one Wm^{-2} of each other.

Last, application of the four methods for converting PIR raw measurements to irradiance was analyzed using several test instruments. The major conclusion of these comparisons suggests that using the Philipona et al. (1995) form, i.e., Eq. (3), consistently does the best as a method to transfer the calibration to field-deployed PIRs. However, the Reda et al. (2002) and Payne and Anderson (1999) coefficients are not available for the calibration standards, which may have led to some of the differences in Fig. 5. For one or two of the six PIR comparisons, such as those in Fig. 3, but not all shown, the Reda et al. (2002) and Payne and Anderson (1999) results were close to the Philipona et al. (1995) results, but not consistently for the six instruments calibrated.

Formatted: Superscript

Deleted: this study

Appendix

An unexpected outcome from fitting thermistor data led us to the following result. If Eq. (7) is used for a least-squares fit of the YSI 44031 data in kiloohms versus a least-squares fit in ohms, i.e., with the quadratic term set to zero, we get the results shown in Fig. 3. The only difference is the data in ohms are divided by 1000 before the fit is made. Recall from above, that if the full cubic in natural log is used there are no distinguishable differences from the blue line in Fig. 2, repeated as a blue line in Fig. 3, whether using ohms or kiloohms.

The requirement of a quadratic term for expressing the Steinhart-Hart equation with kiloohms can be demonstrated by substituting R with units of ohms in Eq. (7) with $1000R_k$, where R_k is in units of kiloohms as shown in Eq. (8).

$$\frac{1}{T} = a + b \cdot ln(1000R_k) + d \cdot ln(1000R_k)^3 \quad (8)$$

Applying logarithm rules to Eq. (8) results in Eq. (9).

$$\frac{1}{T} = a + b\big(ln(1000) + ln(R_k)\big) + d\big(ln(1000) + ln(R_k)\big)^3 \quad (9)$$

Expanding and regrouping terms in Eq. (9) then gives Eq. (10) through Eq. (14).

$$\frac{1}{T} = a_k + b_k \cdot ln(R_k) + c_k \cdot ln(R_k)^2 + d_k \cdot ln(R_k)^3 \quad (10)$$

Formatted: Right: 0.25"

$$a_k = a + b \cdot ln(1000) + d \cdot ln(1000)^3 \quad (11)$$

$$b_k = b + 3d \cdot ln(1000)^2 \quad (12)$$

$$c_k = 3d \cdot ln(1000) \quad (13)$$

$$d_k = d \quad (14)$$

Thus, when data are in kiloohms an equation of the form of Eq. (10) (i.e. full cubic) is required to match the results of Eq. (7) when data are in units of ohms.

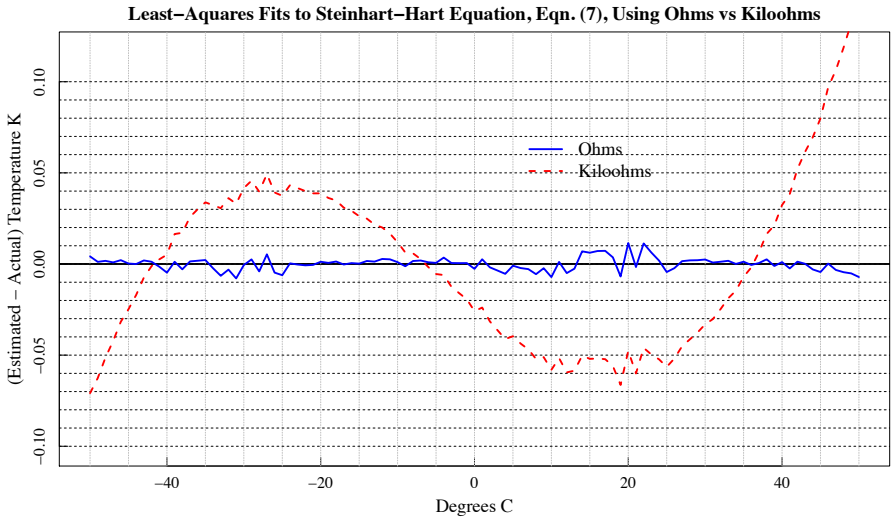

Figure A. Steinhart-Hart equation fit to ohms (blue solid line) versus kiloohms (red dashed line).

References

Albrecht, B. and Cox, S. K.: Procedures for improving pyrgeometer performance, J. Appl. Meteorol., 16, 188-197, https://doi.org/10.1175/1520-0450(1977)016<0190:PFIPP>2.0.CO;2, 1977.

Gröbner, J.: PMOD calibration reports for PIR pyrgeometers, 2024, and private communications.

McArthur, L.: Baseline Surface Radiation Network (BSRN) - Operation Manual Version 2.1 , Ontario, Canada, WMO, p. 68, hdl:10013/epic.52032, 2005.

Formatted: Right: 0.25"

Payne, R.E. and Anderson, S.P.: A new look at calibration and use of Eppley precision infrared radiometers. Part II: calibration and use of the woods hole oceanographic institution improved meteorology precision infrared radiometer J. Atmos. Ocean. Tech., 16, 741-751, https://doi.org/10.1175/1520-0426(1999)016<0739:ANLACA>2.0.CO;2, 1999.

Philipona, R., Frohlich, C., Betz, C.: Characterization of pyrgeometers and the accuracy of atmospheric longwave, Appl. Optics, 34, 1598-1605, https://doi.org/10.1364/AO.34.001598, 1995.

Reda, Ibrahim, Hickey, John R., Stoffel, Tom, and Myers, Daryl: Pyrgeometer calibration at the National Renewable Energy Laboratory (NREL), J. Atmos. Sol.-Terr. Phy., 64, 1623-1629 10.1016/S1364-6826(02)00133-5, 2002.

Steinhart, John S. and Hart, Stanley R.: Calibration curves for thermistors, Deep-Sea Res., 15, 497-503, https://doi.org/10.1016/0011-7471(68)90057-0, 1968

Formatted: Right: 0.25"

Page 6: [1] Deleted	**John Augustine**	**4/29/25 10:29:00 AM**

Page 11: [2] Deleted	**John Augustine**	**4/22/25 1:53:00 PM**

Page 11: [2] Deleted	**John Augustine**	**4/22/25 1:53:00 PM**

Page 11: [2] Deleted	**John Augustine**	**4/22/25 1:53:00 PM**

Page 11: [2] Deleted	**John Augustine**	**4/22/25 1:53:00 PM**

Page 11: [2] Deleted	**John Augustine**	**4/22/25 1:53:00 PM**

Page 11: [2] Deleted	**John Augustine**	**4/22/25 1:53:00 PM**

Page 11: [2] Deleted	**John Augustine**	**4/22/25 1:53:00 PM**

Page 11: [2] Deleted	**John Augustine**	**4/22/25 1:53:00 PM**

Page 11: [2] Deleted	**John Augustine**	**4/22/25 1:53:00 PM**

Page 11: [2] Deleted	**John Augustine**	**4/22/25 1:53:00 PM**

Page 11: [2] Deleted	**John Augustine**	**4/22/25 1:53:00 PM**

Page 11: [2] Deleted	**John Augustine**	**4/22/25 1:53:00 PM**

Page 11: [2] Deleted	**John Augustine**	**4/22/25 1:53:00 PM**

Page 11: [2] Deleted	**John Augustine**	**4/22/25 1:53:00 PM**

Page 11: [2] Deleted	**John Augustine**	**4/22/25 1:53:00 PM**

Page 11: [2] Deleted	**John Augustine**	**4/22/25 1:53:00 PM**

Page 11: [2] Deleted	**John Augustine**	**4/22/25 1:53:00 PM**

Page 11: [2] Deleted	**John Augustine**	**4/22/25 1:53:00 PM**

Page 11: [2] Deleted	**John Augustine**	**4/22/25 1:53:00 PM**
Page 11: [2] Deleted	**John Augustine**	**4/22/25 1:53:00 PM**
Page 11: [2] Deleted	**John Augustine**	**4/22/25 1:53:00 PM**
Page 11: [2] Deleted	**John Augustine**	**4/22/25 1:53:00 PM**
Page 11: [2] Deleted	**John Augustine**	**4/22/25 1:53:00 PM**
Page 11: [2] Deleted	**John Augustine**	**4/22/25 1:53:00 PM**
Page 11: [2] Deleted	**John Augustine**	**4/22/25 1:53:00 PM**
Page 11: [3] Deleted	**John Augustine**	**4/22/25 4:17:00 PM**
Page 11: [3] Deleted	**John Augustine**	**4/22/25 4:17:00 PM**
Page 11: [3] Deleted	**John Augustine**	**4/22/25 4:17:00 PM**
Page 11: [3] Deleted	**John Augustine**	**4/22/25 4:17:00 PM**
Page 11: [3] Deleted	**John Augustine**	**4/22/25 4:17:00 PM**
Page 11: [3] Deleted	**John Augustine**	**4/22/25 4:17:00 PM**
Page 11: [3] Deleted	**John Augustine**	**4/22/25 4:17:00 PM**
Page 11: [3] Deleted	**John Augustine**	**4/22/25 4:17:00 PM**
Page 11: [3] Deleted	**John Augustine**	**4/22/25 4:17:00 PM**
Page 11: [3] Deleted	**John Augustine**	**4/22/25 4:17:00 PM**
Page 11: [3] Deleted	**John Augustine**	**4/22/25 4:17:00 PM**

Page 11: [3] Deleted	John Augustine	4/22/25 4:17:00 PM
Page 11: [3] Deleted	John Augustine	4/22/25 4:17:00 PM
Page 11: [3] Deleted	John Augustine	4/22/25 4:17:00 PM
Page 11: [3] Deleted	John Augustine	4/22/25 4:17:00 PM
Page 11: [3] Deleted	John Augustine	4/22/25 4:17:00 PM
Page 11: [3] Deleted	John Augustine	4/22/25 4:17:00 PM
Page 11: [3] Deleted	John Augustine	4/22/25 4:17:00 PM
Page 11: [3] Deleted	John Augustine	4/22/25 4:17:00 PM
Page 11: [3] Deleted	John Augustine	4/22/25 4:17:00 PM
Page 11: [3] Deleted	John Augustine	4/22/25 4:17:00 PM
Page 11: [3] Deleted	John Augustine	4/22/25 4:17:00 PM
Page 11: [3] Deleted	John Augustine	4/22/25 4:17:00 PM
Page 11: [3] Deleted	John Augustine	4/22/25 4:17:00 PM
Page 11: [3] Deleted	John Augustine	4/22/25 4:17:00 PM
Page 11: [3] Deleted	John Augustine	4/22/25 4:17:00 PM
Page 11: [3] Deleted	John Augustine	4/22/25 4:17:00 PM
Page 11: [3] Deleted	John Augustine	4/22/25 4:17:00 PM